Exploring Vessel Wall Biology In Vivo by Ultrasensitive Total-Body PET

Thorsten Derlin[1], Benjamin A. Spencer[2], Martin Mamach[3], Yasser Abdelhafez[4], Lorenzo Nardo[4], Ramsey D. Badawi[2,4], Simon R. Cherry*[2,4], and Frank M. Bengel*[1]

[1]*Department of Nuclear Medicine, Hannover Medical School, Hannover, Germany;* [2]*Department of Biomedical Engineering, University of California, Davis, Davis, California;* [3]*Department of Medical Physics and Radiation Protection, Hannover Medical School, Hannover, Germany; and* [4]*Department of Radiology, University of California, Davis, Davis, California*

Ultrasensitive, high-resolution, extended-field-of-view total-body (TB) PET using the first-of-its-kind 194-cm axial-field-of-view uEXPLORER may facilitate the interrogation of biologic hallmarks of hitherto difficult-to-evaluate low-signal vessel wall pathology in cardiovascular disease. **Methods:** Healthy volunteers were imaged serially for up to 12 h after a standard dose of ^{18}F-FDG ($n = 15$) or for up to 3 h after injection of a very low dose (about 5% of a standard dose; $n = 15$). A cohort undergoing standard ^{18}F-FDG PET ($n = 15$) on a conventional scanner with a 22-cm axial field of view served as a comparison group. Arterial wall signal, crosstalk with hematopoietic and lymphoid organs, and image quality were analyzed using standardized techniques. **Results:** TB PET depicted the large vessel walls with excellent quality. The arterial wall could be imaged with high contrast up to 12 h after tracer injection. Ultralow-dose TB ^{18}F-FDG images yielded a vessel wall signal and target-to-background ratio comparable to those of conventional-dose, short-axial-field-of-view PET. Crosstalk between vessel wall and lymphoid organs was identified with better accuracy in both TB PET cohorts than in conventional PET. **Conclusion:** TB PET enables detailed assessment of in vivo vessel wall biology and its crosstalk with other organs over an extended time window after tracer injection or at an ultralow tracer dose. These initial observations support the feasibility of serial imaging in low-risk populations and will stimulate future mechanistic studies or therapy monitoring in atherosclerosis and other vessel wall pathologies.

Key Words: vessel wall; PET; total-body imaging; inflammation; atherosclerosis

J Nucl Med 2023; 64:416–422
DOI: 10.2967/jnumed.122.264550

Biologic activity of the vessel wall has emerged as an attractive target for noninvasive molecular imaging because of its key role in atherosclerosis (*1*) but also in other vascular pathologies such as vasculitis or aneurysm (*2,3*). Specifically, atherosclerosis is recognized today as an inflammatory disease of the arterial wall, for which progression is linked to a tight interplay with the hematopoietic system and various other systemic factors (*4*).

PET has provided translationally relevant insights into plaque biology; into the crosstalk between vessel wall, hematopoietic system, and other systemic factors; into the importance of biologic systems activation for disease progression; and into the response to pharmacologic intervention (*5–12*). The application of PET in atherosclerosis has still, however, been limited mostly to single or dual time points in an individual, because of the radiation exposure derived from standard tracer doses (*13*). Limited sensitivity for the detection of weak signal from the relatively small vessel-wall target region is considered another challenge, as is the need for sequential imaging of body regions that are not covered by the limited axial field of view of a standard PET scanner.

Total-body (TB) PET is a recent technologic innovation characterized by an extended axial field of view that covers the entire body simultaneously and provides an up to 15–68 times higher detection sensitivity than current conventional PET systems, along with the highest spatial resolution (~3.0 mm) of any current clinical whole-body PET scanner (*14*). The performance characteristics of the first-of-its-kind 194-cm-long TB PET scanner, the uEXPLORER (United Imaging Healthcare), have recently been reported (*15,16*). Its capabilities for imaging of the vessel wall, however, have not yet been investigated. Here, we report the usefulness of TB PET for vascular molecular imaging at high contrast and a very low dose and for simultaneous assessment of systemic interaction with the hematopoietic and lymphoid systems.

MATERIALS AND METHODS

This is a condensed version of the methods; the full version is in the supplemental materials, available at http://jnm.snmjournals.org.

Study Design and Data Collection

This prospective study included 3 different cohorts (total $n = 45$) (Table 1). The first cohort ($n = 15$) included healthy subjects imaged with a standard dose (372 ± 17 MBq) of ^{18}F-FDG on the uEXPLORER TB PET scanner at the University of California, Davis, at 1.5, 3, and 12 h after injection, to determine the feasibility of an extended time window for imaging of the vessel wall. The second cohort ($n = 15$) included healthy subjects imaged with an ultralow dose (19.6 ± 1.7 MBq) of ^{18}F-FDG using the same scanner at 1.5 and 3 h after injection, to determine the potential for disease screening and repeat imaging with minimal radiation to the patient. The third cohort ($n = 15$) included a sex-matched patient group imaged with a standard dose (307 ± 12 MBq) of ^{18}F-FDG using a conventional PET scanner (Fig. 1) with a 22-cm axial field of view (Biograph mCT flow; Siemens Healthineers). Cardiovascular risk factors and medication were documented (*17,18*). The study protocol complied with the Declaration of Helsinki and was approved by the institutional review boards of the University of California, Davis (approval 1341792), and Hannover Medical School

Received Jun. 21, 2022; revision accepted Sep. 28, 2022.
For correspondence or reprints, contact Thorsten Derlin (derlin.thorsten@mh-hannover.de).
*Contributed equally to this work.
Published online Sep. 29, 2022.

TABLE 1
Characteristics of Conventional and TB PET Cohorts

Parameter	Conventional PET cohort	TB PET cohorts	
		Standard dose	Ultralow dose
Subjects (*n*)	15	15	15
Sex (%)			
Male	40	40	53
Female	60	60	47
Age (y)			
Mean ± SD	59.0 ± 10.4	49.7 ± 14.7	45.0 ± 11.1
Range	33–72	26–78	26–62
Body mass index (kg/m^2)			
Mean ± SD	25.3 ± 3.1	29.1 ± 5.7	25.8 ± 3.4
Range	19.9–28.7	19.4–37.0	20.4–32.3
Cardiovascular risk factors			
Arterial hypertension (*n*)	7 (47%)	3 (20%)	1 (7%)
Hypercholesterolemia (*n*)	3 (20%)	5 (33%)	4 (27%)
Diabetes mellitus (*n*)	2 (13%)	0	0
History of smoking (*n*)	9 (60%)	1 (7%)	1 (7%)
Pack-years*			
Mean ± SD	44 ± 22	15	20
Range	10–80		
Prior myocardial infarction (*n*)	4 (27%)	0	0
Prior stroke (*n*)	1 (7%)	0	0
Prior cardiovascular intervention (*n*)	5 (33%)	0	0
Family history of IHD (*n*)	4 (27%)	4 (27%)	5 (33%)
Statin medication (*n*)	7 (47%)	2 (13%)	2 (13%)
Injected dose		3 (20%)	1 (7%)
Mean ± SD	307.2 ± 11.5	372.4 ± 17.0	19.6 ± 1.7
Range	291.1–328.6	337.3–393.8	17.2–23.5

*There was only 1 subject with history of smoking within each of these 2 cohorts; there is no SD and range is equal to the mean.
SD = standard deviation; IHD = ischemic heart disease.
Cardiovascular risk factors were available for 11 subjects in standard-dose cohort and 12 subjects in ultralow-dose cohort and in all patients of conventional cohort.

(approval 8774_BO_S_2019). All patients at the University of California, Davis, and Hannover Medical School provided written informed consent.

PET Image Acquisition and Reconstruction

TB PET. Ultralow-dose TB CT scans (5 mAs; 140 kVp; tube current modulation on; effective dose, ~1 mSv) or low-dose TB CT scans (50 mAs; 140 kVp; tube current modulation on; effective dose, ~10 mSv) were acquired for attenuation and scatter correction. The CT matrix size was 512 × 512 × 828 with 0.977 × 0.977 × 2.344 mm voxels. A static PET scan of the entire body without bed motion was obtained for 20 min starting 90, 180, and 720 min (standard dose only) after injection. The administered dose of ^{18}F-FDG was 372 ± 17 MBq for the standard-dose cohort (n = 15) and 19.6 ± 1.7 MBq for the low-dose cohort (n = 15). Blood glucose was less than 160 mg/dL in all subjects before injection. Studies were reconstructed from list-mode data with vendor-provided software using an iterative algorithm (20 subsets, 4 iterations) incorporating time-of-flight information but no point-spread function correction. The reconstruction matrix was 256 × 256 × 828 with isotropic voxels of 2.344 mm. Studies were corrected for attenuation, scatter, randoms, and dead time. No smoothing was applied to the reconstructed images.

Conventional PET. Low-dose whole-body CT (25 mAs, reference; 120 kV; CARE Dose4D [Siemens Healthcare]; 5-mm slice thickness; pitch, 1.4) was performed. Using continuous bed motion to cover the entire body, a static PET scan was obtained at 60–90 min after administration of 307 ± 12 MBq (range, 291–329 MBq) of ^{18}F-FDG. Blood glucose was less than 120 mg/dL in all patients before injection. Attenuation-corrected studies were reconstructed using Ultra HD (Siemens Healthcare), an iterative algorithm combined with time-of-flight and point-spread function information (2 iterations; 21 subsets; matrix, 200; zoom, 1.0; gaussian filter, 5.0 mm).

Image Analysis

Vessel wall ^{18}F-FDG signal in major arteries (*19*) was analyzed as described previously using the average SUV_{max} and the arterial target-to-background ratio (*20*), yielding a measure for assessment of global

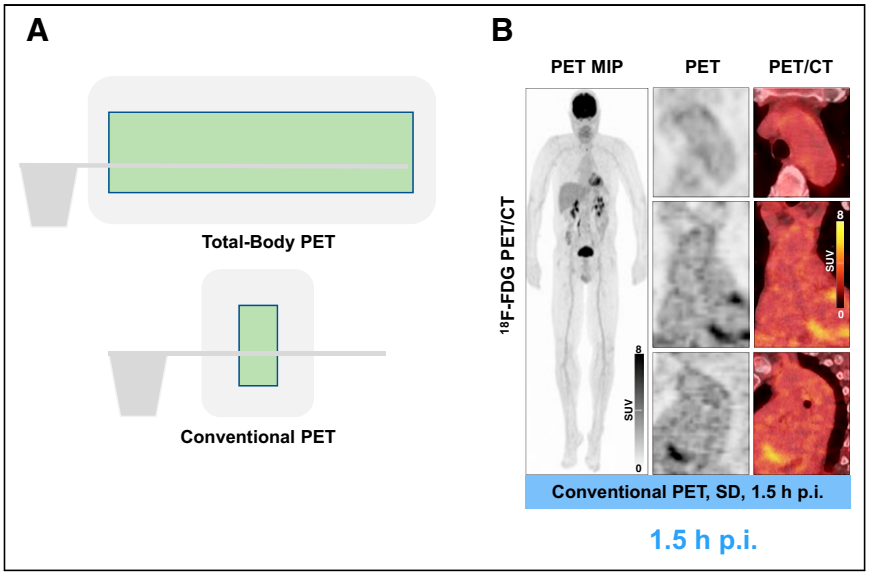

FIGURE 1. Exploring arterial wall biology using ultrasensitive TB PET. (A) Graphical illustration of TB PET scanner vs. conventional short-axial-field-of-view PET scanner. Axial field of view (FOV) of TB PET scanner is 194 cm, providing simultaneous coverage of all tissues and organs in body, with overall increase in effective sensitivity of more than 15- to 68-fold. Axial FOV of conventional PET scanner is typically less than 25 cm. (B) Sample ^{18}F-FDG PET maximum-intensity-projection image and cross-sectional PET and PET/CT images acquired using conventional high-end scanner in 66-y-old man. MIP = maximum-intensity projection; p.i. = after injection; SD = standard dose.

vascular activity for comparison with other surrogate markers of cardiovascular disease (*21*). Likewise, calcified plaque was assessed (*17,19*). For characterization of systemic interactions between arterial wall signal and activity of hematopoietic and lymphoid organs (*10*), spleen signal, bone marrow signal, and lymph node signal were determined. Image noise was assessed using the coefficient of variation of normal liver parenchyma (*22*).

Statistical Analyses

One-way ANOVA with Šídák multiple-comparisons testing, repeated-measures ANOVA with the Geisser–Greenhouse correction and Šídák multiple-comparisons testing, paired *t* tests, and Pearson correlation coefficients were used for analyses. Statistical significance was established for *P* values of less than 0.05. Analysis was performed using Prism (version 9.0; GraphPad Software) for Microsoft Windows.

RESULTS

Subjects in the TB PET cohorts exhibited a significantly lower number of calcified vessel wall lesions than patients in the conventional PET cohort ($P = 0.011$ for standard-dose cohort; $P = 0.002$ for ultralow-dose cohort), consistent with a lower cardiovascular risk profile (Supplemental Tables 1–3; Table 1). However, a clear-cut vessel wall signal was identified by TB PET in these cohorts despite their lower risk profile.

TB PET Allows for High-Contrast Vessel Wall Imaging by Enabling Imaging Much Later After Tracer Injection

Standard-dose TB PET images yielded excellent image quality up to the final time point of 12 h after ^{18}F-FDG injection (Fig. 2). For both the aortic wall and other arterial walls, SUV_{max} as a measure of vessel wall signal strength was comparable between early standard-dose TB PET and conventional PET (Supplemental Table 4), albeit the conventional cohort had a higher risk profile. Arterial wall signal (SUV_{max}) increased significantly at very late imaging (1.5 vs. 12 h after injection: SUV_{max}, $P < 0.0001$) in standard-dose TB PET, whereas there were only minor changes in arterial wall signal between 1.5 and 3 h after injection in both TB cohorts. Importantly, blood-pool signal significantly decreased over time ($P < 0.0001$ in all cases), leading to a significant increase in the target-to-background ratio as a measure of vessel wall contrast ($P < 0.0001$ in all cases). Image noise increased at later imaging time points, particularly (and expectedly) on 12-h delayed images (Supplemental Table 4).

TB PET Imaging of the Vessel Wall Is Feasible Using Ultralow Radiotracer Doses

Ultralow-dose TB PET images were of good quality, providing clear visualization of the vessel wall (Fig. 3). Expectedly, there was more noise than for standard-dose images, but the arterial wall signal strength was comparable, and the target-to-background ratio demonstrated the same temporal evolution toward an increase over time (Fig. 4; Supplemental Table 4).

TB PET Improves Analysis of Interorgan Immune Crosstalk

Signal from spleen and bone marrow (Figs. 5 and 6) did not significantly differ between cohorts (lymph node signal was higher in the ultralow-dose cohort). Regarding intraindividual imaging time points, spleen signal decreased over time ($P \leq 0.0143$), whereas bone marrow signal consistently increased over time (standard dose, $P \leq 0.0017$; ultralow dose, $P = 0.0014$) in both TB PET

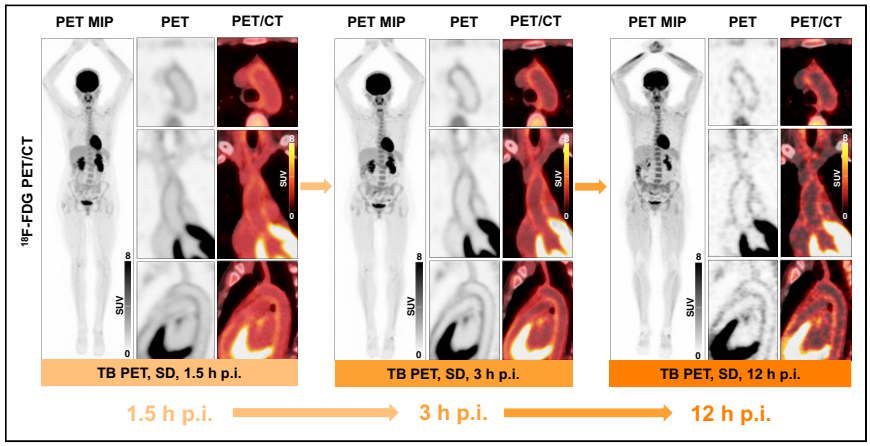

FIGURE 2. Sample TB ^{18}F-FDG PET maximum-intensity-projection images and cross-sectional PET/CT images at different time points using standard radiotracer dose (~370 MBq), ranging from 1.5 h after injection to 12 h after injection. TB PET imaged aortic wall with excellent quality and high contrast, which improved with time. MIP = maximum-intensity projection; p.i. = after injection; SD = standard dose.

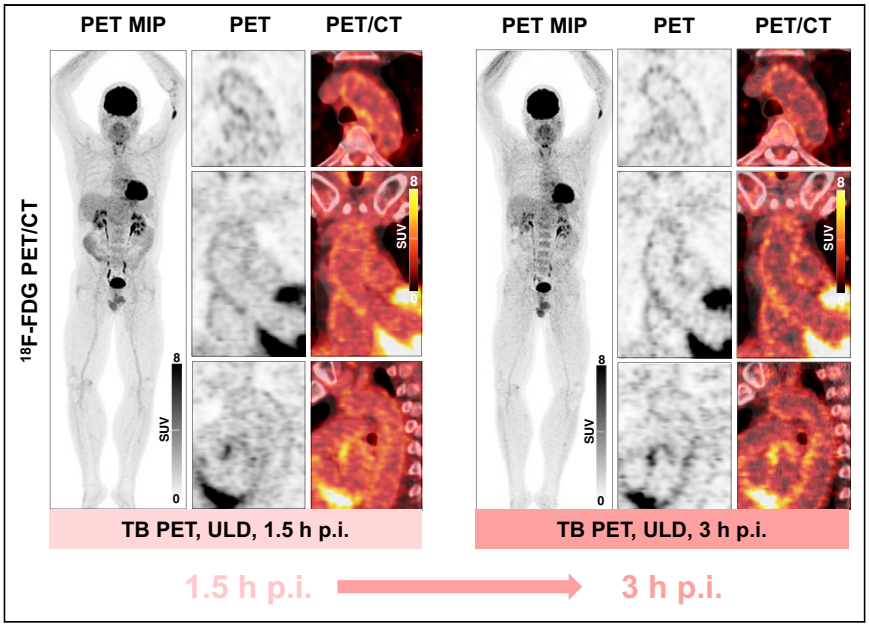

FIGURE 3. Sample TB ^{18}F-FDG PET/CT images at 1.5 and 3 h after injection using very low radiotracer dose (~5% of standard dose). Clear vessel wall signal can be obtained using very low radiotracer doses. MIP = maximum-intensity projection; p.i. = after injection; ULD = ultralow dose.

cohorts (Supplemental Table 5). Importantly, arterial wall signal and activity in lymphoid organs correlated more frequently and more strongly for TB PET than for standard PET (Supplemental Table 6; Fig. 7), particularly in high-quality early images.

DISCUSSION

PET has been used in the past as a powerful tool for noninvasive interrogation of vessel wall biology in vivo. For this use, it has provided valuable insights into disease mechanisms and responses to therapeutic interventions (*5–12*). However, the arterial wall represents a thin target structure, where target molecules and cell types of interest are more difficult to identify than in larger organs and tissues (*10*). Using standard PET scanners, robust signal detection remains challenging and is often restricted to large vascular structures or requires high-end motion correction and extended acquisition techniques (*23*). Our study supports the notion that the recently reported 15- to 68-fold sensitivity gain for TB PET, when compared with current standard systems (*15*), can be used for improved vessel wall imaging. Intriguingly, the sensitivity of TB PET enables delayed and longitudinal imaging after many half-lives of the radionuclide. For the first time, to our knowledge, we have evaluated the evolution of the arterial wall signal up to 12 h after injection of ^{18}F-FDG, equivalent to about 6.5 half-lives of ^{18}F. The vessel wall signal increased significantly over time. And because blood pool continuously clears over time, the vessel wall target-to-background ratio improves further, providing superior contrast. Delayed imaging with optimized contrast is therefore one option resulting from the use of ultrasensitive TB PET. Although the target-to-background ratio increased over time, the time point with the highest SUV in arterial wall imaging could not be determined from this study. Images were acquired not continuously but at certain time points.

Another feasible option supported by our study is the use of ultralow-dose imaging. Radiation exposure may be seen as an obstacle to the application of vascular PET imaging, especially in low-risk populations or for serial observations (*13,24*). The effective dose from a standard activity of 370 MBq of ^{18}F-FDG is about 7 mSv, but using ultralow-dose TB PET, we showed that imaging of the vessel wall is feasible using doses of as low as 5% of a standard dose for up to 3 h after injection, with good image quality and comparable signal strength and vascular contrast compared with standard techniques, although the conventional PET cohort had a higher risk profile, likely associated with a higher true wall signal (*12*). The effective dose of 0.4 mSv for the 20 MBq of ^{18}F-FDG in the ultralow-dose protocol is less than 15% of the natural annual radiation exposure, supporting the feasibility of longitudinal studies or broader cross-sectional applications of this technique. Although additional radiation exposure will originate from the CT scan obtained for anatomic coregistration, we expect that there will be solutions for further dose reduction here, too. We note that with the 5-mAs CT protocol used for TB PET in this study, the estimated dose was only 1 mSv. Given the excellent anatomic detail in the stand-alone TB PET images, it may, for example, be conceivable to perform PET-only studies using artificial intelligence–derived maps for

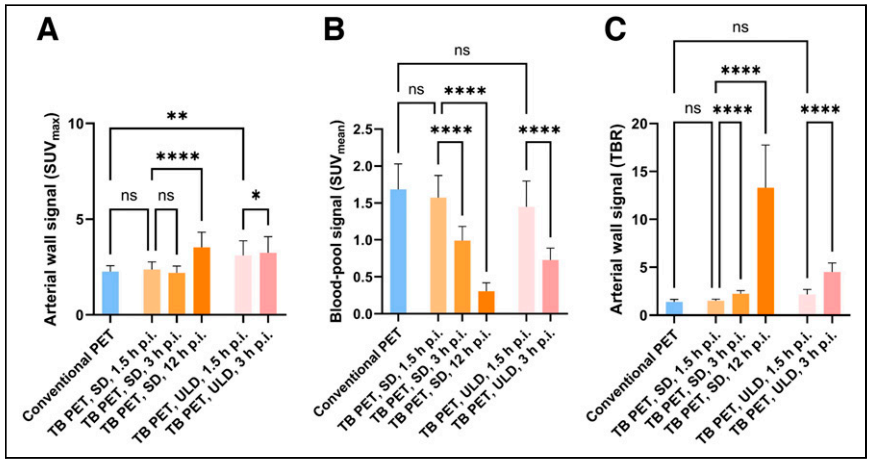

FIGURE 4. Multiple-time-point imaging of arterial wall signal. (A) Arterial wall SUV_{max} increased significantly at very late imaging (12 h after injection, $P < 0.0001$) on standard-dose TB PET, whereas there were only minor changes in arterial wall signal between 1.5 and 3 h after injection in both TB cohorts. (B) By contrast, blood pool SUV_{max} significantly decreased at later imaging time points on TB PET (standard dose, $P < 0.0001$; ultralow dose, $P < 0.0001$). (C) Result was increase in target-to-background ratio over time (standard dose, $P < 0.0001$; ultralow dose, $P < 0.0001$). * – <0.05; ** –<0.01; *** –<0.001; **** –<0.0001. ns = not statistically significant; p.i. = after injection; SD = standard dose; ULD = ultralow dose.

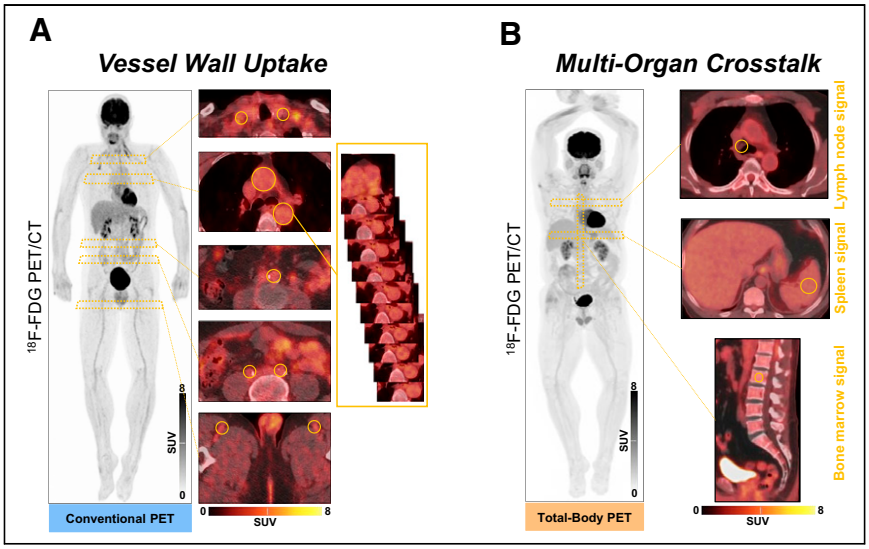

FIGURE 5. Dissecting multiorgan immune crosstalk. (A) Assessment of arterial wall uptake in different large arteries using regions of interest in sample conventional PET. For each arterial localization, uptake was evaluated in 10 slices and then averaged (left panel, PET maximum-intensity-projection image; middle and right panels, transaxial PET/CT images). (B) Sample TB ^{18}F-FDG PET maximum-intensity-projection image (left panel) and cross-sectional PET/CT images (right panel) used for assessment of multiorgan networks.

attenuation correction of PET images (*25*). Last, further reduction of injected activity was not tested in our study but appears possible if early imaging time points are used. Nevertheless, a detailed analysis of distinct plaques would likely require a higher CT image quality (and dose) for an appropriate analysis of individual plaque structure. Furthermore, we assessed the global vascular activity (*21*) but not the activity of individual plaques. Analysis of distinct arterial plaques is particularly difficult—and may be less reliable—in the presence of image noise. Importantly, there was more noise using ultralow radiotracer doses than for the standard-dose images in this study, highlighting the need for higher tracer doses when analyzing distinct plaques.

Unlike conventional PET, which is acquired with sequential bed positions alternating between image acquisition and patient table motion, TB PET allows for simultaneous imaging of the entire body, providing a superior measurement technique without changes in tracer distribution due to varying imaging time points for different parts of the body. This not only enables accurate and complete coverage of the whole vascular tree but also provides simultaneous information from other organs and tissues that may be interconnected. Our study showed that TB PET may provide more robust information on the relationship between vessel wall signal and activated lymphoid system than standard PET. Simultaneous coverage of the entire body may therefore be superior for analysis of systems-based interactions. The complex, multifaceted systemic interactions between cardiovascular disease and other organs or tissues have gained increasing interest and fostered the emergence of novel interdisciplinary clinical subspecialities such as neurocardiology, cardiorheumatology, and cardiooncology (*8,26,27*). An example is that the local inflammatory tissue response after acute myocardial infarction not only may result in a systemic inflammatory response with exacerbated vessel wall inflammation (*28*) but also induces neuroinflammation as a potential precursor to cognitive dysfunction (*29*). TB PET holds the key to providing further and deeper insights into these interorgan interactions at the crossroads between cardiovascular medicine and other fields.

The potential of TB PET for vascular imaging may grow even further. The ultrahigh sensitivity will enable ultrafast imaging (*30,31*), which can be used to obtain parametric images after pixelwise kinetic modeling (*32*) and may enable real-time motion correction of moving structures such as the coronary arteries. Dynamic TB imaging allows for generation of parametric images using voxel-based Patlak graphical analysis, such as of the metabolic rate of ^{18}F-FDG. Absolute quantification of arterial wall signal and hematopoietic and lymphoid organ signal may show further improved characterization of systemic organ interactions compared with standard SUV images (*33*). Such advanced technical developments are expected to yield an even further increase in contrast and accuracy. Additionally, it is important to recognize that although ^{18}F-FDG was used as a tracer example in this study, the methods can be transferred to any other PET tracer. ^{18}F-FDG has been validated as a marker of plaque inflammation (*34*) but has also been shown to have specificity limitations (*7*). Other clinically feasible tracers, such as ^{18}F-sodium fluoride (*7,17*) or ^{68}Ga-pentixafor (*19,23*), may benefit equally from the advantages of TB PET.

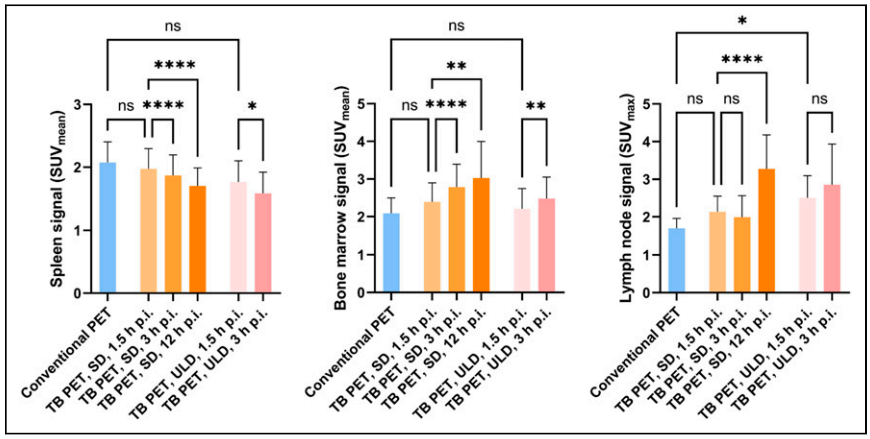

FIGURE 6. Dissecting multiorgan immune crosstalk. Spleen and bone marrow signal did not significantly differ between conventional PET and TB PET cohorts. Regarding intraindividual imaging time points, spleen signal decreased over time (e.g., standard-dose TB PET at 12 h after injection [$P < 0.0001$]), whereas bone marrow signal increased with time (standard dose, $P \leq 0.0017$; ultralow dose, $P = 0.0014$) in both TB PET cohorts. Lymph node signal increased significantly at 12 h after injection ($P < 0.0001$). * − <0.05; ** − <0.01; *** − <0.001; **** − <0.0001. ns = not statistically significant; p.i. = after injection; SD = standard dose; ULD = ultralow dose.

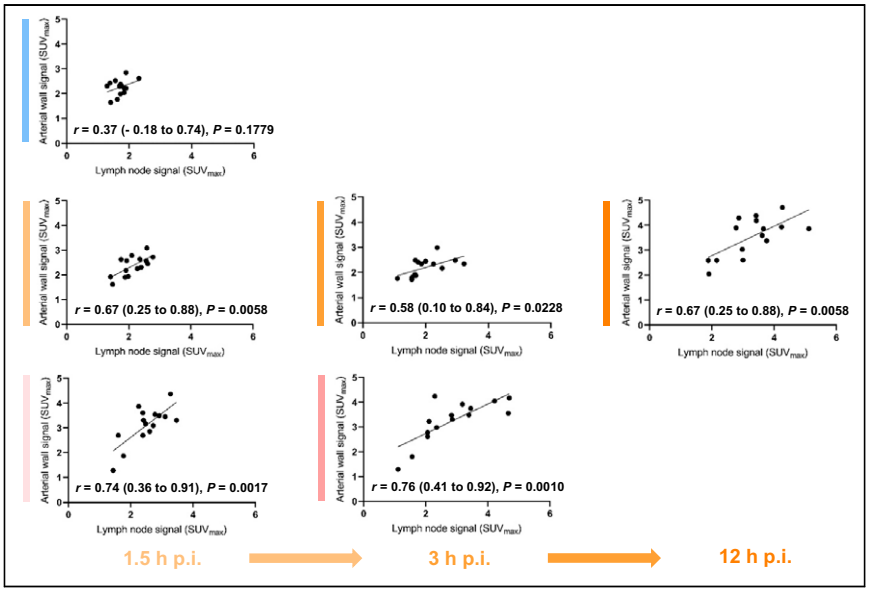

FIGURE 7. Dissecting multiorgan immune crosstalk. Arterial wall signal does not correlate with lymph node signal in conventional PET cohort (top row). By contrast, correlation is significant and consistent in both TB PET cohorts (middle and bottom rows), both at early imaging time points (left column) and at delayed imaging (middle and right columns).

Some limitations of our work should be acknowledged. First, the sample size in the different cohorts was limited, and the TB PET cohorts comprised healthy volunteers with a predominantly low cardiovascular risk profile, precluding a meaningful analysis of the association between arterial wall signal and cardiovascular risk factors in the context of low statistical power to detect such associations. Although imaging of large cohorts of volunteers remains challenging, future analyses may comprise larger clinical samples of patients scanned with TB PET, once the technology has been more broadly applied. Biologic (e.g., the different accepted blood glucose values at the time of PET) and technical factors affecting SUVs may have influenced the study results to some extent but reflect different clinical practices at different sites contributing patients to this study. However, the aim of this study was to demonstrate both principal novel applications and the improved characterization of biologic processes using TB PET. Future studies may also demonstrate an improved relation between PET signal and histopathologic ground truth, that is, inflammation in cases of ^{18}F-FDG (*34*) or with other inflammatory biomarkers such as C-reactive protein. In particular, correlation with biomarkers may improve at later acquisition times (e.g., at 12 h after injection) and with an optimized target-to-background situation, which might be worthwhile exploring. We provided a first indication of such an improved characterization of biologic processes, given the better correlation between vessel wall signal and hematopoietic and immune organ activity such as spleen and regional lymph nodes in TB PET. Finally, this work focused on demonstrating the initial feasibility of vessel wall imaging using the uEXPLORER scanner, but it was not designed as a controlled trial, such as to monitor the effects of a specific pharmacologic intervention. Our work provides the technologic basis for such studies and should be seen as a stimulus for future more expansive efforts.

CONCLUSION

The first human vessel wall imaging studies using the ultrasensitive, high-resolution TB PET uEXPLORER system highlight the opportunities for extended-time-window imaging, ultralow-dose imaging, and systems-based analysis of interorgan interaction. Future work will focus on further advances in TB PET data analysis, on additional vessel wall–targeted radiopharmaceuticals, and on clinical feasibility studies using TB PET for such applications as atherosclerosis screening with a global disease activity score, imaging-based stratification for therapy, and repeat imaging in treatment monitoring.

DISCLOSURE

Grant funding was received from the German Research Foundation (BE2217/6-1) and the National Institutes of Health (R01 CA206187). The University of California, Davis, has a revenue-sharing agreement and a research agreement (principal investigators, Ramsey Badawi and Simon Cherry) with United Imaging Healthcare. No other potential conflict of interest relevant to this article was reported.

ACKNOWLEDGMENTS

We are grateful for the invaluable expertise and support of the technologists and clinical research staff involved in this study.

KEY POINTS

QUESTION: Does TB PET improve imaging of vessel wall activity in patients with atherosclerosis?

PERTINENT FINDINGS: TB PET enabled detailed assessment of in vivo vessel wall biology and its crosstalk with other organs, over an extended time window after tracer injection or at an ultralow tracer dose.

IMPLICATIONS FOR PATIENT CARE: TB PET may influence the present clinical practice of cardiovascular PET imaging. These initial observations support the feasibility of serial imaging in low-risk populations, and they will stimulate future mechanistic studies or therapy monitoring in atherosclerosis and other vessel wall pathologies.

REFERENCES

1. Daghem M, Bing R, Fayad ZA, et al. Noninvasive imaging to assess atherosclerotic plaque composition and disease activity: coronary and carotid applications. *JACC Cardiovasc Imaging.* 2020;13:1055–1068.
2. Slart RHJA, Writing Group, Reviewer Group, et al. FDG-PET/CT(A) imaging in large vessel vasculitis and polymyalgia rheumatica: joint procedural recommendation of the EANM, SNMMI, and the PET Interest Group (PIG), and endorsed by the ASNC. *Eur J Nucl Med Mol Imaging.* 2018;45:1250–1269.
3. Malm BJ, Sadeghi MM. Multi-modality molecular imaging of aortic aneurysms. *J Nucl Cardiol.* 2017;24:1239–1245.
4. Libby P. The changing landscape of atherosclerosis. *Nature.* 2021;592:524–533.
5. Werner RA, Bengel FM, Derlin T. Emerging molecular targets for imaging of atherosclerotic plaque using positron emission tomography. *Curr Radiopharm.* 2021;14:173–183.
6. Fayad ZA, Mani V, Woodward M, et al. Safety and efficacy of dalcetrapib on atherosclerotic disease using novel non-invasive multimodality imaging (dal-PLAQUE): a randomised clinical trial. *Lancet.* 2011;378:1547–1559.

7. Joshi NV, Vesey AT, Williams MC, et al. ^{18}F-fluoride positron emission tomography for identification of ruptured and high-risk coronary atherosclerotic plaques: a prospective clinical trial. *Lancet.* 2014;383:705–713.
8. Tawakol A, Ishai A, Takx RA, et al. Relation between resting amygdalar activity and cardiovascular events: a longitudinal and cohort study. *Lancet.* 2017;389: 834–845.
9. Keliher EJ, Ye YX, Wojtkiewicz GR, et al. Polyglucose nanoparticles with renal elimination and macrophage avidity facilitate PET imaging in ischaemic heart disease. *Nat Commun.* 2017;8:14064.
10. van der Valk FM, Kuijk C, Verweij SL, et al. Increased haematopoietic activity in patients with atherosclerosis. *Eur Heart J.* 2017;38:425–432.
11. Chowdhury MM, Tarkin JM, Albaghdadi MS, et al. Vascular positron emission tomography and restenosis in symptomatic peripheral arterial disease: a prospective clinical study. *JACC Cardiovasc Imaging.* 2020;13:1008–1017.
12. Singh P, Emami H, Subramanian S, et al. Coronary plaque morphology and the anti-inflammatory impact of atorvastatin: a multicenter ^{18}F-fluorodeoxyglucose positron emission tomographic/computed tomographic study. *Circ Cardiovasc Imaging.* 2016;9:e004195.
13. Meinel FG, Nance JW Jr, Harris BS, et al. Radiation risks from cardiovascular imaging tests. *Circulation.* 2014;130:442–445.
14. Cherry SR, Badawi RD, Karp JS, et al. Total-body imaging: transforming the role of positron emission tomography. *Sci Transl Med.* 2017;9:eaaf6169.
15. Badawi RD, Shi H, Hu P, et al. First human imaging studies with the EXPLORER total-body PET scanner. *J Nucl Med.* 2019;60:299–303.
16. Spencer BA, Berg E, Schmall JP, et al. Performance evaluation of the uEXPLORER total-body PET/CT scanner based on NEMA NU 2-2018 with additional tests to characterize PET scanners with a long axial field of view. *J Nucl Med.* 2021;62:861–870.
17. Derlin T, Wisotzki C, Richter U, et al. In vivo imaging of mineral deposition in carotid plaque using ^{18}F-sodium fluoride PET/CT: correlation with atherogenic risk factors. *J Nucl Med.* 2011;52:362–368.
18. Subramanian S, Emami H, Vucic E, et al. High-dose atorvastatin reduces periodontal inflammation: a novel pleiotropic effect of statins. *J Am Coll Cardiol.* 2013;62: 2382–2391.
19. Weiberg D, Thackeray JT, Daum G, et al. Clinical molecular imaging of chemokine receptor CXCR4 expression in atherosclerotic plaque using ^{68}Ga-pentixafor PET: correlation with cardiovascular risk factors and calcified plaque burden. *J Nucl Med.* 2018;59:266–272.
20. Derlin T, Koenecke C, Schultze-Florey C, et al. CD19-targeted immunotherapy attenuates vessel wall inflammation. *JACC Cardiovasc Imaging.* 2021;14:1864–1866.
21. Bucerius J, Hyafil F, Verberne HJ, et al. Position paper of the Cardiovascular Committee of the European Association of Nuclear Medicine (EANM) on PET imaging of atherosclerosis. *Eur J Nucl Med Mol Imaging.* 2016;43:780–792.
22. Yan J, Schaefferkoette J, Conti M, et al. A method to assess image quality for low-dose PET: analysis of SNR, CNR, bias and image noise. *Cancer Imaging.* 2016; 16:26.
23. Derlin T, Sedding DG, Dutzmann J, et al. Imaging of chemokine receptor CXCR4 expression in culprit and nonculprit coronary atherosclerotic plaque using motion-corrected [^{68}Ga]pentixafor PET/CT. *Eur J Nucl Med Mol Imaging.* 2018;45:1934–1944.
24. Everett BM, MacFadyen JG, Thuren T, et al. Inhibition of interleukin-1β and reduction in atherothrombotic cardiovascular events in the CANTOS trial. *J Am Coll Cardiol.* 2020;76:1660–1670.
25. Arabi H, Bortolin K, Ginovart N, et al. Deep learning-guided joint attenuation and scatter correction in multitracer neuroimaging studies. *Hum Brain Mapp.* 2020;41: 3667–3679.
26. Mantel Ä, Holmqvist M, Andersson DC, et al. Association between rheumatoid arthritis and risk of ischemic and nonischemic heart failure. *J Am Coll Cardiol.* 2017;69:1275–1285.
27. Campia U, Moslehi JJ, Amiri-Kordestani L, et al. Cardio-oncology: vascular and metabolic perspectives: a scientific statement from the American Heart Association. *Circulation.* 2019;139:e579–e602.
28. Dutta P, Courties G, Wei Y, et al. Myocardial infarction accelerates atherosclerosis. *Nature.* 2012;487:325–329.
29. Thackeray JT, Hupe HC, Wang Y, et al. Myocardial inflammation predicts remodeling and neuroinflammation after myocardial infarction. *J Am Coll Cardiol.* 2018;71:263–275.
30. Zhang X, Xie Z, Berg E, et al. Total-body dynamic reconstruction and parametric imaging on the uEXPLORER. *J Nucl Med.* 2020;61:285–291.
31. Zhang X, Cherry SR, Xie Z, Shi H, Badawi RD, Qi J. Subsecond total-body imaging using ultrasensitive positron emission tomography. *Proc Natl Acad Sci USA.* 2020;117:2265–2267.
32. Wang G, Nardo L, Parikh M, et al. Total-body PET multiparametric imaging of cancer using a voxel-wise strategy of compartmental modeling. *J Nucl Med.* 2022; 63:1274–1281.
33. Derlin T, Werner RA, Weiberg D, Derlin K, Bengel FM. Parametric imaging of biologic activity of atherosclerosis using dynamic whole-body positron emission tomography. *JACC Cardiovasc Imaging.* 2022;15:2098–2108.
34. Rudd JH, Warburton EA, Fryer TD, et al. Imaging atherosclerotic plaque inflammation with [^{18}F]-fluorodeoxyglucose positron emission tomography. *Circulation.* 2002;105:2708–2711.